International Journal of GEOMATE, April, 2024 Vol.26, Issue 116, pp.11-18
ISSN: 2186-2982 (P), 2186-2990 (O), Japan, DOI: https://doi.org/10.21660/2024.116.4113
Geotechnique, Construction Materials and Environment

CAPACITY TESTING OF REINFORCED CONCRETE BEAMS USING POST-ULTIMATE LOAD GFRP-S REINFORCEMENT

*Arbain Tata[1], Mufti Amir Sultan[2] and Fikram Selang[3]

[1,2,3] Civil Engineering Department, Khairun University, Indonesia

*Corresponding Author, Received: 02 Sep. 2023, Revised: 14 Feb. 2024, Accepted: 29 Feb. 2024

ABSTRACT: The ultimate load is known as the ultimate strength of a structure. It is the maximum load a structure can withstand before collapsing. Structural reinforcement is needed for structures experiencing low strength due to dead load, live load, fatigue load, and earthquakes. In this research, Glass Fiber Reinforced Polymer (GFRP) shows a highly viable solution because of its benefits, encompassing exceptional corrosion resistance, lightweight properties, high strength, ease of installation, and commendable durability. This research aimed to compare the three sample groups to evaluate the effect of GFRP on reinforced concrete beams. The collected data included assessments of maximum load and deflection. Test specimens were constructed in three sets of distinct variations. The first set comprised concrete beams reinforced without GFRP, designated as control beams (BN), totaling three pieces. The second set entailed concrete beams reinforced with GFRP, labeled as BG. The third variation consisted of reinforced concrete beams subjected to collapse or post-ultimate load conditions and subsequently strengthened with GFRP, labeled as BGPU. The purpose is to observe the influence of GFRP-S reinforcement on reinforcing three beams. The analysis showed that direct GFRP-reinforced beams exhibited load increases ranging from 13.59% to 29.76% compared to control beams. In the case of post-ultimate load GFRP reinforcement, load enhancements of 6.80% to 16.78% were observed. These results showed the potential of GFRP reinforcement in repairing damaged beams, providing a viable solution for structural enhancement.

Keywords: Structure, Beams, GFRP-S, Ultimate Load

1. INTRODUCTION

The concept of structural ultimate load, also known as ultimate strength, is the maximum load a structure can withstand before collapsing. Building structures are frequently susceptible to damage, particularly the ones caused by seismic events. Certain structures encountered excessive loading conditions induced by dynamic forces such as fatigue or seismic activities [1, 2]. In addition to the challenges posed by aging and variations in load, earthquake-induced damage can manifest as cracking, spalling, delamination, and, in the worst-case scenario, building collapse. Addressing these issues becomes imperative to prevent structural failures and ensure the safety of standing constructions. In engineering, significant advancements have led to the emergence of fiber-reinforced polymer (FRP) as a viable material solution for structural reinforcement and repair. The overarching goal of the reinforcement is to restore or enhance the strength of elements to withstand anticipated loads. Several studies, such as encasement with concrete [3, 4], encasement with steel [5, 6], and encasement with lightweight composite materials, particularly FRP, were used for the achievement of structural reinforcement [7, 8, 9]. FRP constitutes a composite material characterized by a polymer resin matrix reinforced with glass or carbon fibers. The use of FRP materials for reinforcing concrete is gaining significant favor due to a list of advantages, including its lightweight material [10], remarkable tensile strength [11, 12], corrosion resistance [13], commendable durability [14], ease of installation, dimensional stability [15], and straightforward maintenance [16].

Several studies explored the application of Glass Fiber Reinforced Polymer (GFRP) in beams. For instance, an investigation showed that externally bonded GFRP sheets offered an effective means to augment the strength of reinforced concrete beams and enhance their load-carrying capacity [17, 18]. Beams reinforced with FRP exhibit heightened stiffness and yield ultimate strength. In another study centered on rehabilitating corroded reinforcement in beams, GFRP was used for flexural reinforcement in concrete beams, yielding load increases of 75.15% and substantial improvements in maximum deflection [19]. Additionally, finite element simulations focusing on using GFRP-S as external reinforcement have indicated that the sheets can significantly enhance the flexural capacity of reinforced concrete beams compared to those lacking GFRP-S reinforcement [20, 21]. FRP has been developed in various forms, such as grids, rods, sheets, and plates. It is most commonly used due to its relatively lower cost than

the other FRP materials. A visual appearance of FRP in the form of a Glass Fiber Reinforced Polymer - Sheet is depicted in Figure 1.

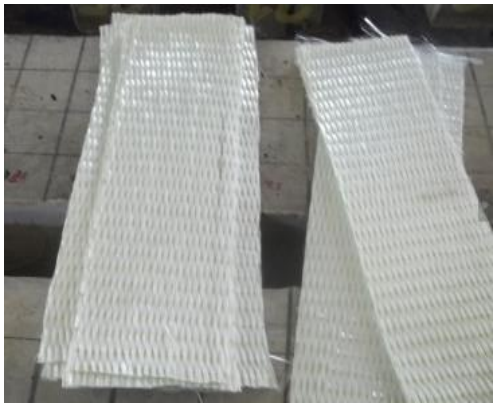

Fig. 1 Glass Fiber Reinforced Polymer - Sheet

This study aims to comprehensively explore the behavior of reinforced concrete structures that experience collapse and subsequently undergo reinforcement using GFRP. The overarching goal is to achieve an analysis of the effects of GFRP reinforcement on concrete following this catastrophic event. Glass Fiber Reinforced Polymer (GFRP) shows a highly viable solution because of its benefits, encompassing exceptional corrosion resistance, lightweight properties, high strength, ease of installation, and commendable durability.

2. RESEARCH SIGNIFICANCE

Numerous studies have examined the reinforcement of beam elements in building structures, which significantly differed from post-ultimate load reinforcement investigations. Certain structures encountered excessive loading conditions induced by dynamic forces such as fatigue or seismic activity. These events could lead to structural collapses, necessitating costly demolition and the subsequent construction of new buildings, resulting in significant economic expenses and environmental pollution. However, some buildings held the potential for repair and strengthening to continue serving their intended purposes. This study aimed to evaluate the impact of applied reinforcement on cracked beam structures that had gone through ultimate load conditions but still exhibited the potential goal of restoring their functionality. In North Maluku, a powerful earthquake measuring 7.20 on the Richter scale caused extensive damage to several office and commercial buildings. Before embarking on repair efforts for these structures, it was crucial to conduct a comprehensive study to ascertain the potential strength improvements achievable using GFRP-S reinforcement. In this particular case, GFRP-S material had been selected for its affordability and accessibility.

3. STUDY METHODOLOGY

The experimental tests were conducted within the Structure and Materials Laboratory of the Engineering Program, Faculty of Engineering, Khairun University. This study has involved the examination of 3 (three) normal concrete beams, 3 (three) concrete beams reinforced with GFRP, and 3 (three) cracked concrete beams reinforced with GFRP.

Table 1 Reinforcing steel tensile test results.

Diameter of bar	Yield of bar (MPa)	Maximum stress (MPa)	Tensile/elastic modulus (GPa)
ø 8	240.50	417.20	15.00

The reinforcement process encompassed the application of epoxy resin as an adhesive between the beams and layers of GFRP sheets, serving as flexural reinforcement. Detailed information regarding the materials used for each test specimen can be seen in Tables 1 and 2.

Table 2 Specifications for GFRP-S type SHE51 (Fyfe. Co LLC)

Properties of fiber materials	
Properties	Test value
Tensile stress (GPa)	3.24
Tensile modulus (GPa)	72.40
Maximum Strain (%)	4.50
Weight per area (gr/cm^2)	915.00
Fiber sheet thickness (mm)	0.36

In this study, the installation of GFRP-S was conducted by using the wet lay-up method, which involves a manual application of FRP by hand. The process began with the preparation of an epoxy resin mixture, applied to the concrete surface. After the epoxy had reached the appropriate consistency, it was evenly distributed across the concrete using a brush or roller. Subsequently, GFRP was positioned on the concrete surface. A critical consideration during this process was the prevention of air entrapment between the glass fibbers and the beams. To ensure that no air was trapped, pressure should be applied using hands or a roller on the GFRP layer. This step was essential to guarantee the thorough saturation of resin, preventing any air from becoming trapped.

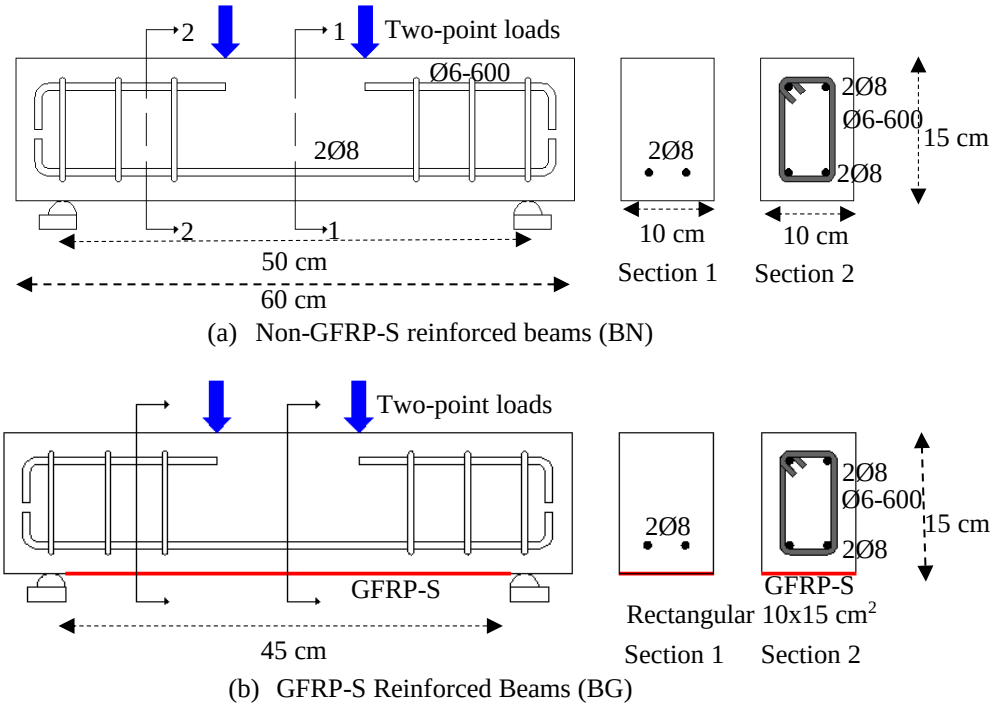

Fig. 2 GFRP-Reinforced Beams (a) BN; and (b) BG

3.1 Test Stages

The setup for the beam's flexural strength test is shown in Figure 2. A total of 10 samples were manufactured, including three reinforced concrete beams, three concrete beams reinforced with GFRP, three cracked concrete beams reinforced with GFRP, and one non-reinforced concrete beam. Each beam possessed dimensions of 10 x 15 x 60 cm.
The test was conducted through a flexural strength test apparatus employing a Point Load configuration until the beams reached the ultimate load. Cracked beams were grouted and filled with cement paste before being reinforced with GFRP-S on the tensile side. Subsequently, the beams reinforced with GFRP-S were subjected to test until collapse occurred. Flexural reinforcement with FRP, design calculations referred to ACI committee 440.2R-08 [22] is shown in Figures 3.

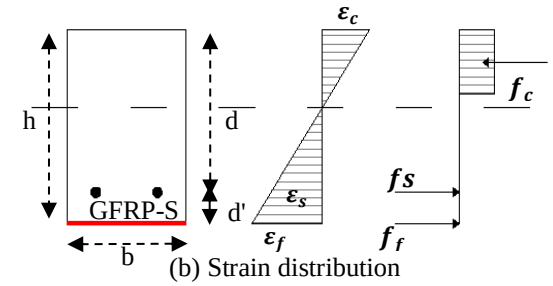

Fig. 3 Elastic strain and stress distribution.

These calculations are presented in the following formulas. The moment capacity (M_n) on the beam is obtained from the coupling action between the concrete compressive force (C) and the tensile force GFRP-S (t_f). The moment arm (c) is the moment arm connecting the two forces is the value determined first.

$$\emptyset Mn \geq Mu \quad (1)$$

$$k_m = \frac{1}{60\ \varepsilon_{fu}} \left(1 - \frac{n\,E_f\,t_f}{360.000}\right) \leq 0{,}90 \quad (2)$$

$$\varepsilon_{fe} = \varepsilon_{cu}\left(\frac{h-c}{c}\right) - \varepsilon_{bi} \leq k_m \varepsilon_{fu} \quad (3)$$

$$f_{fe} = E_f \varepsilon_{fe} \quad (4)$$

$$\varepsilon_s = \varepsilon_{fe} + \varepsilon_{bi}\left(\frac{d-c}{h-c}\right) \quad (5)$$

$$f_s = E_s \varepsilon_s \leq f_y \quad (6)$$

$$C = \frac{A_s f_s + A_f f_{fe}}{\gamma\, f'_c\, \beta 1\, b} \quad (7)$$

$$\boldsymbol{M_n = A_s f_s \left(d - \frac{\beta 1\, c}{2}\right) + \psi_f A_f f_{fe} \left(h - \frac{\beta 1 c}{2}\right)} \quad (8)$$

4. RESULT AND DISCUSSION

4.1 Fine Aggregate Test Results

Fine aggregates used in this study were sourced from Togafo Village, Ternate City, and consists of beach sand. A recapitulation of the fine aggregate test results is shown in Table 3. Aggregate

gradations are shown in Figure 4. The graph shows that the material used meets the terms and conditions for concrete materials. Fine aggregate material is included in zone 2 with a maximum aggregate size of sieve number between 0.15-10 mm. Coarse aggregate material falls into zone 1 with a sieve number between 4.8-40 mm. Recapitulation of fine aggregate and coarse aggregate test results shows results under *Standard Nasional Indonesia* (SNI) specifications.

Coarse aggregates used in this study were obtained from Kali Oba Sofifi, Tidore City. Various characteristics of this aggregate were evaluated, including mud content, water content, aggregate water absorption, oven-dry specific gravity, water-saturated surface dry specific gravity, apparent specific gravity, aggregate fineness modulus, and wear or abrasion. The gradations of coarse and fine aggregates are shown in Figures 4a and 4b. The results of the Kalumata coarse aggregate characteristic test are also summarized in Table 3.

4.2 Coarse Aggregate Test Results

Table 3 Recapitulation of fine aggregate and coarse aggregate test results

Test Type	Fine aggregate test results	SNI Specifications	Coarse aggregate test results	SNI Specifications	Remarks
Water content (%)	1.03	0.2 – 5.0	0.67	0.2 – 1.0	Fulfill
Aggregate water content (%)	3.15	3.0 – 5.0	1.00	0.5 – 2.0	Fulfill
Aggregate water absorption (%)	1.53	0.2 – 2.0	1.35	0.2 – 4.0	Fulfill
Oven-dry specific gravity (gr/cm^3)	2.54	1.6 – 3.2	2.56	1.6 – 3.2	Fulfill
Water-saturated surface dry specific gravity (gr/cm^3)	2.58	1.6 – 3.2	2.60	1.6 – 3.2	Fulfill
Apparent specific gravity (gr/cm^3)	2.64	1.6 – 3.2	2.65	1.6 – 3.2	Fulfill
Fineness modulus (%)	2.51	1.5 – 3.8	6.71	5.0 – 8.0	Fulfill
Wear/abrasion (%)	-	-	1.00	< 40	Fulfill

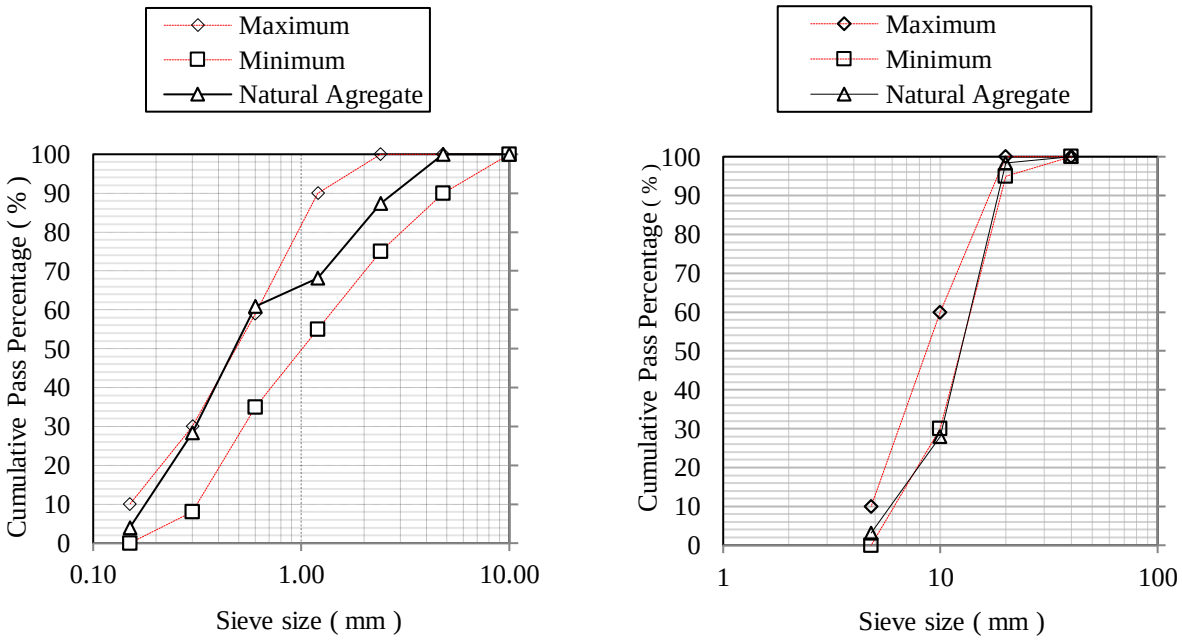

(a) Fine aggregate

(b) Coarse aggregate

Fig. 4 Gradations of fine and coarse aggregates (a) fine aggregate; and (b) Coarse aggregate

4.3 Concrete Job Mix Design

The laboratory conducted aggregate tests to determine the concrete mix proportions for cement, coarse aggregate, fine aggregate, and water in the concrete mix design in achieving 25 MPa concrete strength. In this study, the mix design adhered to SNI 03-2834-2000. The calculated composition of the concrete constituents required for one m³ of mortar at a concrete quality of 25 MPa is shown in Table 4. The composition of this mixture is a reference in determining the mixing of reinforced concrete beams.

Table 4 Composition of the quality mix is 25 MPa

Material Requirements	Weight (Kg/m^3)	Ratio to Cement
Cement	512.50	1.00
Sand	563.14	1.10
Crushed Stone	1044.36	2.04
Water	205.00	0.04
Total	2325.00	

4.4 Compressive Strength Results

The compressive strength of concrete after 28 days of curing was evaluated through cylinder compressive strength assessments. These assessments involved three cylindrical specimens examined using the Compression Strength Test. The results indicated an average compressive strength of 25.52 MPa for the concrete. A summary of the compressive strength test results is shown in Table 5.

Table 5 Summary of compressive strength test results

Sample	Concrete Weight (Kg)	Compressive Strength (MPa)	Average (MPa)
BN 1	12.280	24.25	
BN 2	12.660	26.12	25.52
BN 3	12.380	25.95	

4.5 Flexural Strength Test Result

Flexural strength is a significant property of concrete to be sought out in the research. The flexural strength of concrete beams without reinforcement is shown in Table 6. The formula employed for calculating the strength is written in Eq. (9):

$$f_r = \frac{Pl}{bh^2} \quad (9)$$

Where f_r is the Modulus of rupture; P = load (Force) at the fracture point; l = Length of the support (outer) span; b = width beams; and h = height beams.

Table 6 Modulus of rupture calculation results

Width (b) (mm)	Height (h) (mm)	Length (L) (mm)	Load (P) (N)	Modulus of rupture (MPa)
100	150	450	15000	3

4.6 Load-Deflection Relationship of BN, BG, and BGPU Concrete Beams

The load-deflection relationship derived from the test results is shown in Figure 6. According to Figure 6, BN 1, BN 2, and BN 3 exhibited maximum load values of 40.46 kN, 42.25 kN, and 42.75 kN, along with deflections of 2.05 mm, 2.10 mm, and 2.12 mm, respectively.

The initial crack became visible at a load of 4.0 kN in the sample test results, suggesting the concrete had reached the cracked stage. This signified that the concrete had surpassed its tensile strain capacity, leading to the development of hairline cracks in the flexural region of the beams.

BG 1, BG 2, and BG 3 exhibited maximum load became apparent at loads of 52.50 kN, 47.75 kN, and 50.00 kN, along with deflections of 2.56 mm, 2.52 mm, and 2.54 mm, respectively. For BG 1, BG 2, and BG 3, the initial crack became apparent at loads of 5.0 kN, 4.5 kN, and 4.7 kN, respectively These results indicated that the concrete had exceeded its tensile strain limit, signifying the activation of reinforcement and GFRP-S in bearing tensile forces.

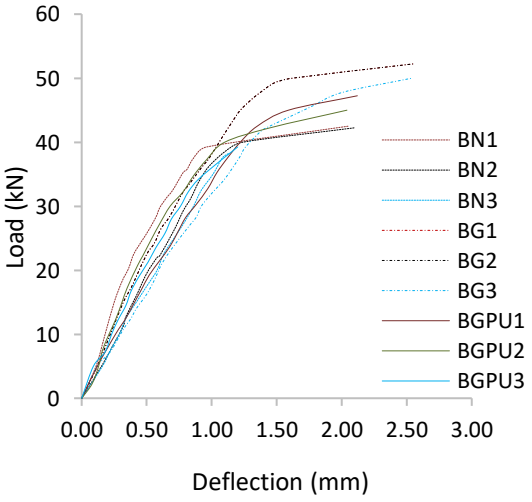

Fig. 6 Load vs Deflection Relationship of the BN, BG, and BGPU.

BGPU 1, BGPU 2, and BGPU 3 exhibited maximum load became apparent at loads of 47.25, 45,00 kN, and 47.75 kN, along with deflections of 2.12 mm, 2.04 mm, and 2.09 mm, respectively. These results indicated that the concrete had exceeded its tensile strain limit, signifying the activation of reinforcement and GFRP-S in bearing tensile forces.

Based on Figure 6, in testing the BGPU 1 beam, there was an increase in the peak load on the BN 1 beam to 16.78 %. At first, the BN 1 beam reached a peak load of 40.46 tons; after that, grouting was carried out by cement paste on the cracked parts and then reinforced with GFRP-S and called the BGPU 1 beam a peak load of 47.25 tons. Likewise, the BGPU 2 beam had the same thing happen to the BN2 beam. The load increased from 42.25 tons initially; after strengthening GFRP-S, the load increased to 45.00 tons. BGPU 3 also experienced an increase in load, initially 42.75 tons. After being strengthened by GFRP-S, the load increased to 47.75 tons. The three test objects showed similar behavior. So, it can be concluded that certain cracked beams can still be utilized by grouting and then strengthening with GFRP, as in this study.

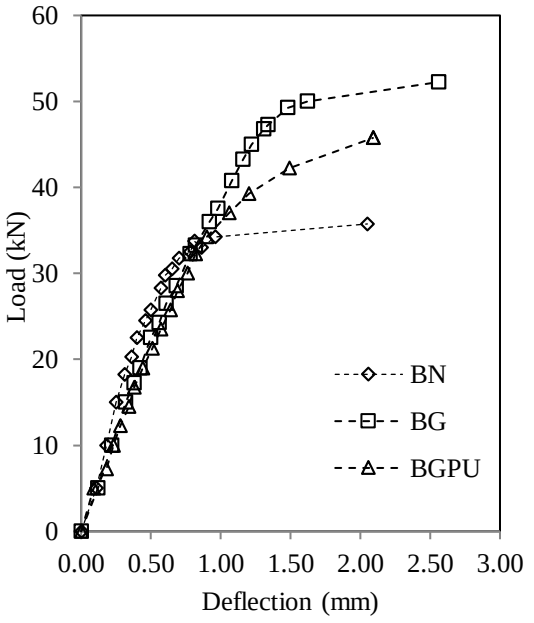

Fig. 7 Load-Deflection Relationship of the BN-BG-BGPU.

Fig. 7 provides a clear comparison of beam strength under different loading conditions. GFRP-reinforced beams showed a significant 29.75% increase in strength compared to the non-GFRP-reinforced counterparts. Meanwhile, cracked beams reinforced with GFRP experienced a 6.80% strength improvement compared to the non-GFRP reinforced part. These results emphasized GFRP reinforcement's effectiveness for beams that have experienced cracking.

4.7 Analysis Results of Maximum Load and Nominal Moment

Calculation and analysis were employed to determine the beam specimens' maximum load and nominal moment values. A summary of the assessment for maximum load and nominal moment in both GFRP-reinforced and non-GFRP-reinforced sections is presented in Table 7.

Table 7 Recapitulation of nominal moment analysis

Specimen	P_{max} Experimental (kN)	P_{max} Finite Element (kN)	Nominal Moment (kN.m)
BN	40.46	40.91	3.54
BG	52.50	53.11	4.81
BGPU	47.25	46.20	4.16

4.8 Collapse Pattern in Beams

The crack patterns observed during the test indicated a flexural crack pattern. These flexural cracks originated from the bottom of the beam cross-section, typically at its mid-span, and propagated upwards in response to increased load or elevated stress caused by bending moments. The crack pattern observed in the beams is depicted in the figure below.

The result of the experimental study and analysis of failure modes are shown in Fig. 8a, 8b, and 8c. The analysis showed that the initial crack in the non-GFRP reinforced section occurred at a load of 40 kN, whereas in the GFRP-reinforced area, it occurred at a pack of 45 kN. This initial crack was characterized by hairline cracks, indicating that the tensile strain capacity of the concrete had been exceeded.

The strain had a small value (0.003 mm) that could not be directly observed. Therefore, the occurrence of the initial crack was based on the analysis of the concrete cracking behavior. The calculation for the non-GFRP reinforced beams showed that the initial crack occurred at a load of 39 kN.

The results of the numerical study and analysis of damaget models in finite element are shown in Fig. 8a, 8b, and 8c [23]. Models are created for BN-FE, BG-FE, and BGPU-FE having different maximum loads of 40.91 kN, 53.11 kN, and 46.20 kN. along with deflections of 2.00 mm, 2.15 mm, and 2.11 mm, respectively. Performed for based on the model analysis results, finite elements for control beams (BN-FE), concrete beams reinforced with GFRP (BG-FE), and concrete beams reinforced with GFRP after ultimate load (BGPU-

FE) show cracks similar to valid experimental results.

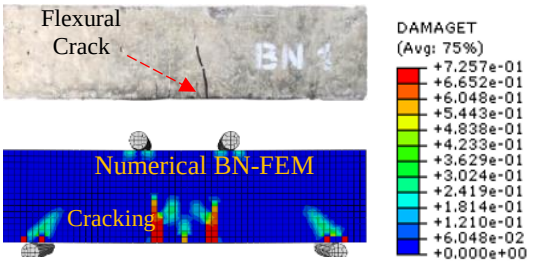

a. Control beams (BN).

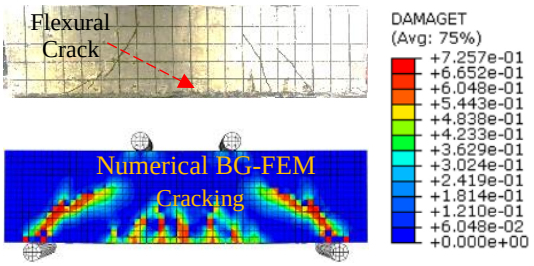

b. Concrete beams reinforced with GFRP (BG).

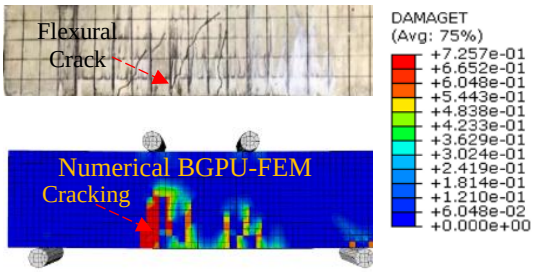

c. BGPU Concrete beams reinforced with GFRP after ultimate load.

Fig. 8 Failure mode and contours of average strain in the transverse direction for specimens BN, BG, and BGPU beams.

5. CONCLUSIONS

In conclusion, the direct reinforcement of beams with GFRP showed a substantial increase in flexural strength of up to 17.64%. Additionally, GFRP reinforcement applied to cracked beams resulted in an 8.43% increase in flexural strength. This indicated that beams with cracks could still be effectively reinforced, with direct reinforcement proving to be more effective in enhancing the strength.

The load-deflection relationship in beams reinforced with GFRP provided valuable insights. Direct GFRP reinforcement substantially elevated the load-carrying capacity by 13.59% to 29.75% and deflection augmentations of 27.85% to 34.21%. Post-ultimate load GFRP reinforcement, on the other hand, led to load increases of 6.80% to16.78% and deflection increases of 11.18% to 18.62%. Although the load-deflection values of post-ultimate load GFRP-reinforced beams were lower than those directly reinforced with GFRP, they still significantly outperformed the control beams.

6. ACKNOWLEDGMENTS

We thank all the parties who contributed to the research, particularly PT. Wijaya Karya Maraja, for the provision of GFRP SE-H51 materials, to all who have assisted the researchers in this research, and to the staff of the Structural and Material Laboratory of the Department of Civil Engineering, Khairun University.

7. REFERENCES

[1] Djamaluddin R., Irmawaty R., and Tata A., Flexural Capacity of Reinforced Concrete Beams Strengthened Using GFRP Sheet after Fatigue Loading for Sustainable Construction, Key Enggineering Material, vol. 692, 2016, pp. 66–73.

[2] Tata A., Parung H., Tjaronge W., and Djamaluddin R., Ultimate Experiment of Ruptured Concrete Beams Strengthened Using GFRP-Sheet after Fatigue Loads, International Journal of Engineering and Technology, vol. 7, no. 1, 2015, pp. 45–49.

[3] Raval S. S., and Dave U. V., Effectiveness of Various Methods of Jacketing for RC Beams, in Procedia Engineering, 51, 2013, pp. 230–239.

[4] Blikharskyy Z., RC Beams Strengthened by RC Jacketing Under Load, Acta Scientiarum Polonorum, vol. 20, no. 1, 2021, pp. 25–30.

[5] Elhamed A., Retrofitting and Strengthening of Reinforced Concrete Damaged Beams Using Jacketing of Steel Wire Mesh with Steel Plates, International Journal of Engineering Research & Technology (IJERT), vol. 4, no. 4, 2015, pp. 596–604.

[6] Thermou G. E., and Elnashai A. S., Seismic Retrofit Schemes for RC Structures and Local-Global Consequences, Progress in Structural Engineering and Materials, vol. 8, no. 1, 2006, pp. 1–15, 2006.

[7] Gemi L., Madenci E., Özkılıç Y. O., Yazman Ş., and Safonov A., Effect of Fiber Wrapping on Bending Behavior of Reinforced Concrete Filled Pultruded GFRP Composite Hybrid Beams, Polymers (Basel), vol. 14, no. 18, 2022, pp. 1–20.

[8] Kashwani G., Al-Tamimi A. K., and Al-Ameri R., Evaluation of FRP Concrete Compression

Member Under Repeated Load And Harsh Environment, International Journal of Geomate, vol. 9, no. 2, 2015, pp. 1460–1466.
[9] Tahmouresi B., Momeninejad K., and Mohseni E., Flexural Response of FRP-Strengthened Lightweight RC Beams: Hybrid Bond Efficiency of L-Shape Ribbed Bars and NSM Technique, Archives of Civil and Mechanical Engineering, vol. 22, no. 2, 2022, pp. 1–16.
[10] Korotkov R., Vedernikov A., Gusev S., Alajarmeh O, Akhatov I., and Safonov A., Shape Memory Behavior of Unidirectional Pultruded Laminate, Composites Part A: Applied Science and Manufacturing, vol. 150, 2021, pp. 1–10, Nov. 2021.
[11] Vedernikov A., Safonov A., Tucci F., Carlone P. and Akhatov I., Pultruded Materials and Structures: A Review, Journal of Composit Material, 2020, pp. 1–37.
[12] Ozutok A., Madenci E. and Kadioglu F., Free Vibration Analysis of Angle-Ply Laminate Composite Beams by Mixed Finite Element Formulation Using the Gâteaux Differential, Science and Engineering of Composite Materials, vol. 21, no. 2, 2014, pp. 257–266.
[13] Aribas U. N., Ermis M., Eratli N., and Omurtag M. H., The Static and Dynamic Analyses of Warping Included Composite Exact Conical Helix by Mixed FEM, Composites Part B: Engineering, 2019, pp. 1–32.
[14] Özütok A. and Madenci E., Free Vibration Analysis of Cross-Ply Laminated Composite Beams by Mixed Finite Element Formulation, International Journal of Structural Stability and Dynamics, vol. 13, no. 2, 2013, pp. 1–18.
[15] Vedernikov A., Nasonov Y., Korotkov R., Gusev S., Akhatov I., and Safonov A., Effects of Additives on the Cure Kinetics of Vinyl Ester Pultrusion Resins, Journal of Composite Material, 2021, pp. 1–17.
[16] Vedernikov A., Safonov A., Tucci, F. Carlone P. and Akhatov I., Modeling Spring-In of l-Shaped Structural Profiles Pultruded at Different Pulling Speeds, Polymers (Basel), vol. 13, no. 16, 2021, pp. 1–26, Aug. 2021.
[17] Sallal, A. K. and Rajan, A., Flexural Behavior of Reinforced Concrete Beams Strengthening with Glass Fiber Reinforced Polymer (GFRP) at Different Sides, International Journal of Science and Research (IJSR), vol. 5, no. 5, 2016, pp. 1837–1843.
[18] Sultan M. A., Djamaluddin R., Tjaronge W., and Parung H., Flexural Capacity of Concrete Beams Strengthened Using GFRP Sheet After Seawater Immersion, in Procedia Engineering, 2015, pp. 644–649.
[19] Soudki K. A., Sherwood T., and Masoud S., FRP Repair of Corrosion-Damaged Reinforced Concrete Beams, Proceedings of the 3rd fib International Congress – 2010, 2010, pp. 1–13.
[20] Michael M. and Leman S., Performance Analysis of Reinforced Concrete Beam with GFRP Using Finite Element Method, International Journal of Application on Sciences, Technology and Engineering, vol. 1, no. 1, 2023, pp. 75–84.
[21] Meena A., Devi K. S., and Sharma A. S., Study on Behaviour of Deep Beam Strengthened with GFRP sheets, in Journal of Physics: Conference Series, IOP Publishing Ltd, Oct. 2021.
[22] ACI 440 2R-08, Guide for The Design and Construction of Externally Bonded FRP Systems for Strengthening Concrete Structures. American Concrete Institute, 2008, pp. 1-76.
[23] N. Y. N. Arya, "Second-order FE Analysis of Axial Loaded Concrete Members According to Eurocode 2," Civ. Archit. Eng., vol. Master, p. 100, 2015, [Online]. Available: http://www.diva-portal.se/smash/get/diva2:828128/FULLTEXT01.pdf.